

Supplementary material

Viscoacoustic wave equations for the power law dependence of Q on frequency

Qi Hao^{1,*}, Stewart Greenhalgh^b

^a*College of Geoexploration Science and Technology, Jilin University, Changchun, 130026, China*
^b*Institute of Geophysics, ETH Zurich, Zurich, 8092, Switzerland*

Abstract

This document provides the supplementary material for the RSPA manuscript “Hao, Q., and S. Greenhalgh. 2021 Viscoacoustic wave equations for the power law dependence of Q on frequency: Proceedings of the Royal Society A: Mathematical, Physical and Engineering Sciences, submitted for peer review”. The RSPA manuscript is abbreviated as HG2021 throughout this document for brevity. This document consists of three parts. The first part shows results in an earthquake frequency band, which is a supplement to the figures in HG2021. This part includes (1) a phase-velocity comparison between the exact and nearly power law frequency-dependent Q dissipative models and (2) numerical modeling for wave propagation in the Marmousi model. By contrast, the second part shows results in an exploration frequency band. It includes (1) a comparison between the dissipative models; (2) numerical examples of viscoacoustic wave propagation. The last part shows explicit expressions for equations A5 through A7 of Appendix A of HG2021.

Keywords: seismic, viscoacoustic, dissipative, wave, power law, frequency dependent, Q

Part one: results in an earthquake-seismology frequency band

In this part, we show supplementary figures to the numerical examples of HG2021. All the model parameters for the examples of this part are the same as those in the corresponding examples of HG2021.

A phase-velocity comparison between the dissipative models

The subsection “(d) A comparison between the dissipative models” in the second section of HG2021 compares the quality factors for the exact and nearly power law frequency-dependent Q dissipative model (equation 2.2 and equations 2.5 and 2.14 in HG2021). Using the model parameters listed in that subsection, we compute the phase velocities for these dissipative models. The formula for the phase velocity is given by $V = [(v_R^2 + v_I^2)/v_R]^{1/2}$, where $v_R - i\text{sgn}(\omega)v_I$ is the complex velocity of a homogeneous plane wave in a dissipative medium. Figures 1 through 4 show a comparison between the phase velocities for these dissipative models. The phase velocities for the nearly power law frequency-dependent Q models approach the exact ones with increasing the series expansion order N (see equations 2.5 and 2.14 in HG2021).

*Corresponding author

Email addresses: xqi.hao@gmail.com (Qi Hao), gstewart@retired.ethz.ch (Stewart Greenhalgh)

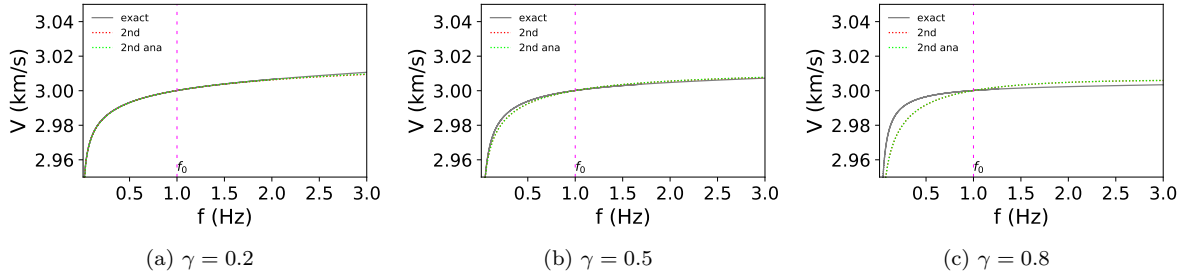


Figure 1: Variation of the quality factors with frequency. The legend label “exact” corresponds to equation 2.2 in HG2021. The legend labels “2nd” and “2nd ana” correspond to equations 2.5 and 2.14 with $N = 2$ in HG2021, respectively.

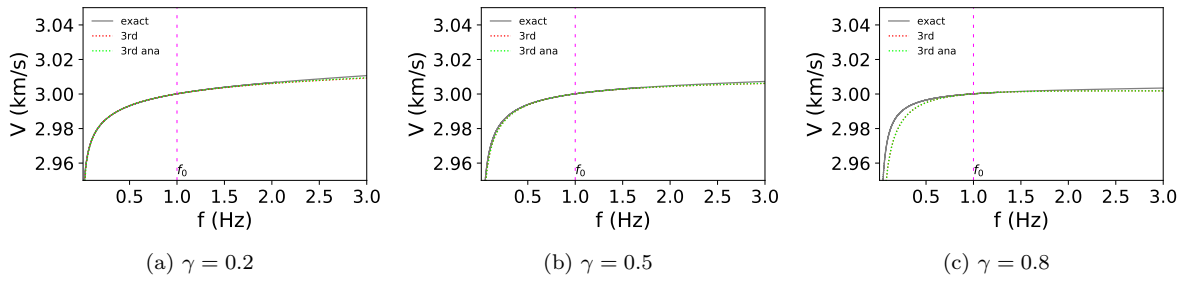


Figure 2: Similar to Figure 1 but using equations 2.5 and 2.14 with $N = 3$ in HG2021.

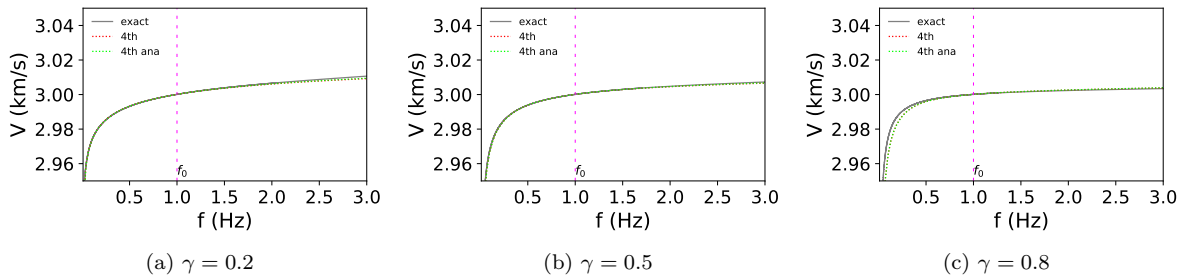


Figure 3: Similar to Figure 1 but using equations 2.5 and 2.14 with $N = 4$ in HG2021.

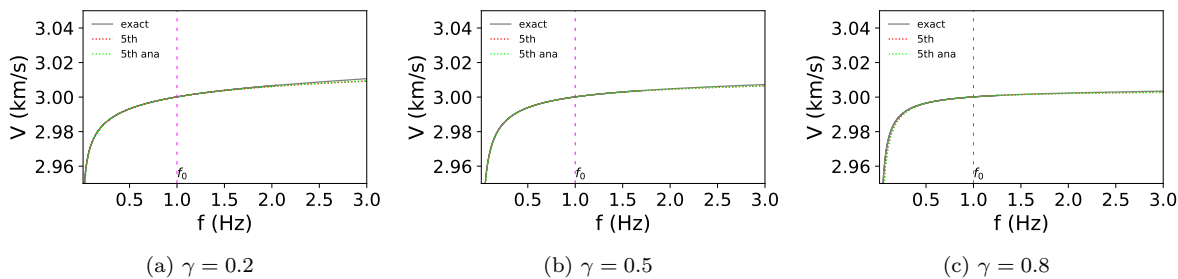


Figure 4: Similar to Figure 1 but using equations 2.5 and 2.14 with $N = 5$ in HG2021.

Numerical modeling for wave propagation in the Marmousi model

This section shows supplementary figures to the second numerical example in the section "Numerical examples of viscoacoustic wave propagation" of HG2021. These figures are produced via the same model parameters and wave equations as those in that section of HG2021. Figure 5 shows the 1 Hz Ricker wavelet and its amplitude spectrum. Figure 6 shows the seismograms for the acoustic, constant Q , and power law frequency-dependent Q versions of the Marmousi model, respectively. A comparison between these seismograms indicates that high frequency components of the viscoacoustic waves are attenuated significantly in particular for the late arrivals (i.e., those waves with traveltimes larger than 50 s). Figures 7 through 12 support the analysis mentioned in HG2021 on the single-trace seismograms, namely that the non-zero exponent parameter γ for the power law frequency-dependent Q affects viscoacoustic waveforms only at a large wave-propagation distance.

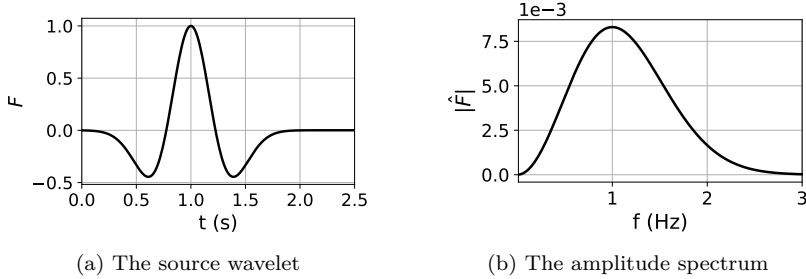


Figure 5: The ricker wavelet and its amplitude spectrum. The dominant frequency is $f_c = 70$ Hz.

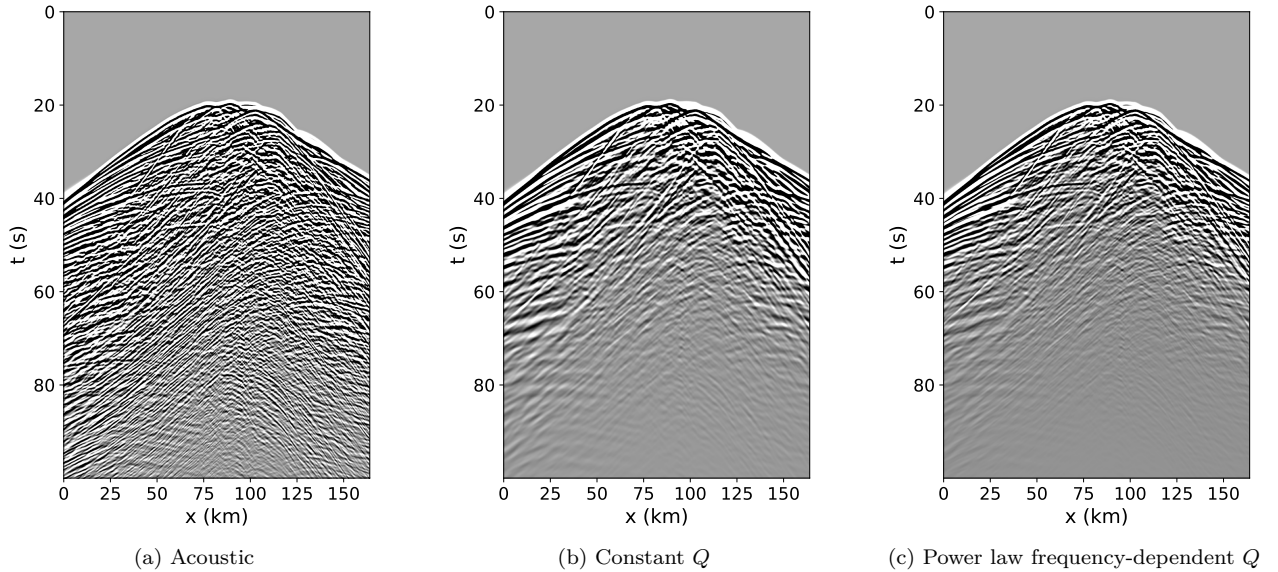


Figure 6: A comparison between the shot-gather seismograms from the acoustic ($Q_0 = \infty$), constant Q ($\gamma = 0$), and power law frequency-dependent Q wave equations, respectively. A gain function $t^{0.4}$ is applied to the seismograms.

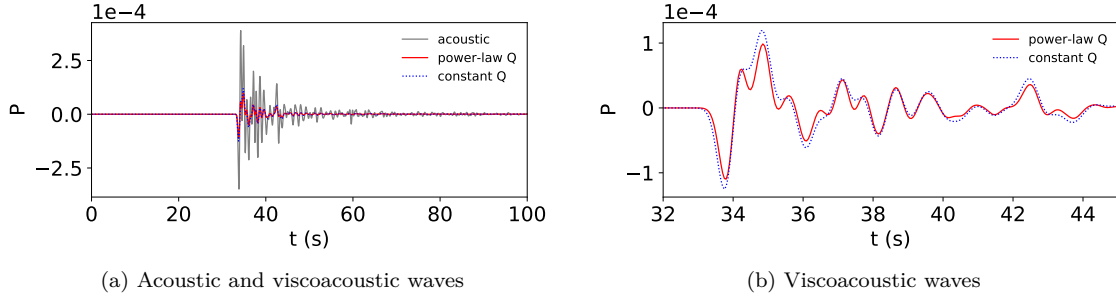


Figure 7: Single-trace seismograms for the receiver at $x = 20$ km. The legend labels “acoustic”, “constant Q ” and “power law Q ” correspond to the acoustic, constant Q and power law frequency-dependent Q cases, respectively. Plots (a) and (b) show the same viscoelastic waveforms at different illustration scales.

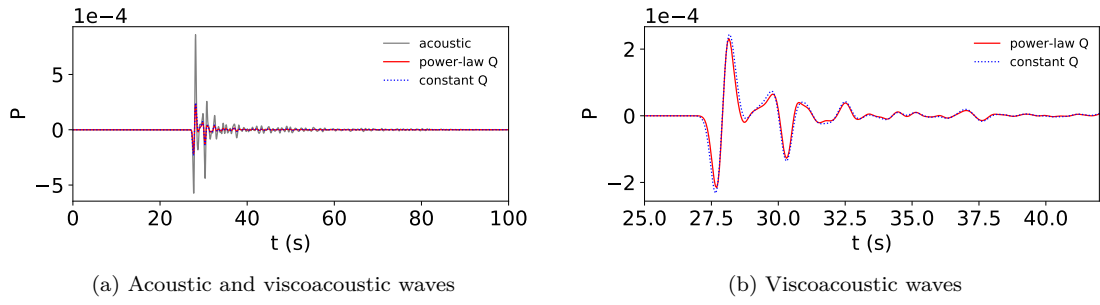


Figure 8: Similar to Figure 7 but for the receiver at $x = 40$ km.

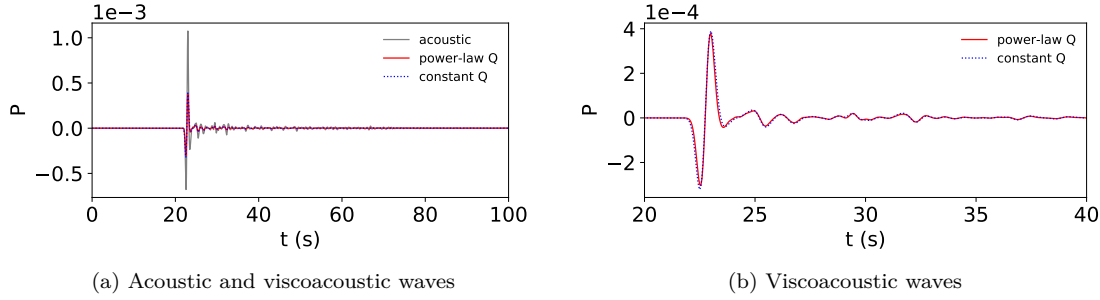


Figure 9: Similar to Figure 7 but for the receiver at $x = 60$ km.

Part two: results in an exploration-seismology frequency band

The HG2021 entirely shows the numerical examples for waves in an earthquake-seismology frequency band. As a supplement, this part shows numerical examples in an exploration-seismology case.

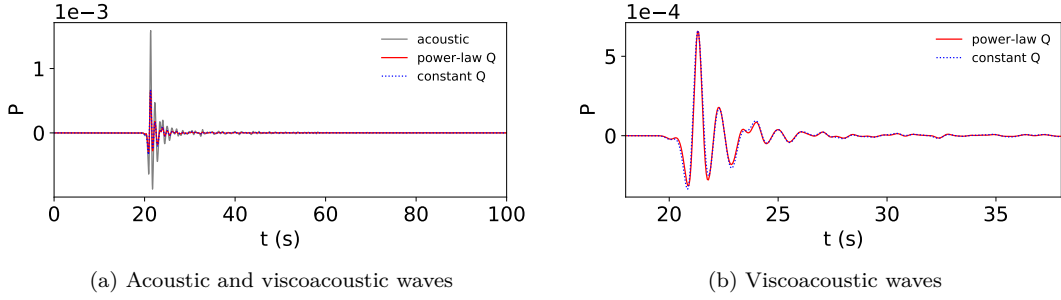


Figure 10: Similar to Figure 7 but for the receiver at $x = 104$ km.

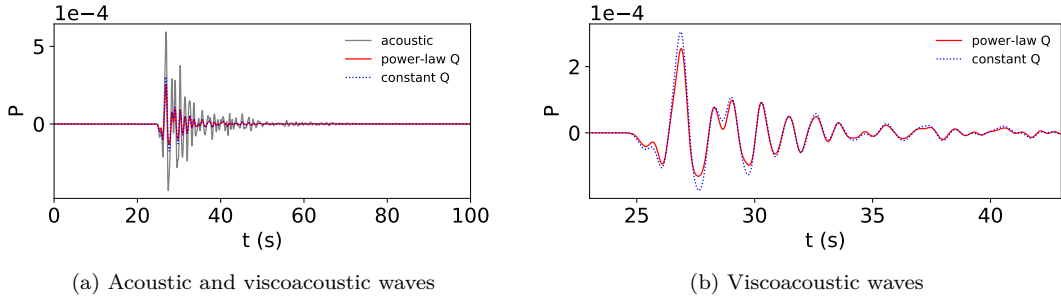


Figure 11: Similar to Figure 7 but for the receiver at $x = 124$ km.

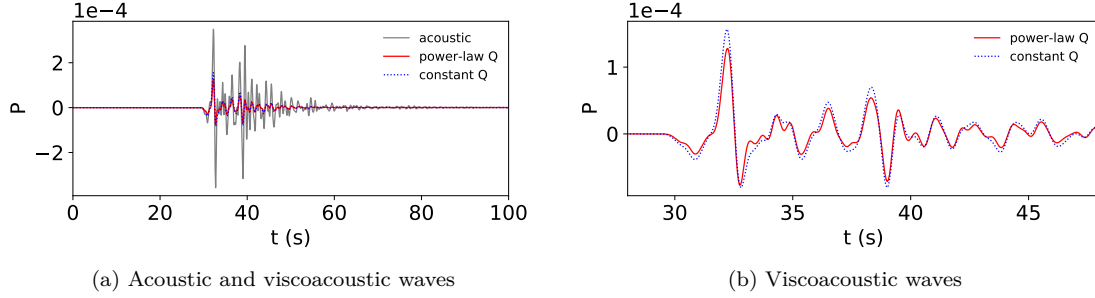


Figure 12: Similar to Figure 7 but for the receiver at $x = 144$ km.

A comparison between the power law frequency-dependent Q dissipative models

We compute the quality factors and phase velocities for the exact and nearly power law frequency-dependent Q dissipative models (equation 2.2 and equations 2.5 and 2.14 in HG2021) in an exploration seismology case ([1, 200] Hz). The relaxation times for the weighting function (equation 2.13 of HG2021) are shown in Table 1. The valid frequency range for the weighting function is [2, 400] Hz, which can cover most of the frequency range of interest ([1, 200] Hz) and can decrease errors in the quality factor at high frequencies for a large exponent parameter γ from our experience. The reference frequency, velocity and quality factor are set as $f_0 = 70$ Hz, $v_0 = 3$ km/s and $Q_0 = 50$, respectively. The exact quality factor and phase velocity are used as a benchmark to analyze the accuracy of our dissipative models. The exact quality factor is obtained from equation 4 of HG2021. The exact phase velocity is obtained from the quality factor dispersion using the Kramers-Kronig relations via the Hilbert

transform to numerically compute equation 4 of [1]. The exponent of the power law Q is set as $\gamma = 0.2, 0.5$ and 0.8 , which represent the weak, moderate and strong frequency-dependence of Q , respectively. As illustrated in Figures 13 through 16, the quality factors for the nearly power law frequency-dependent Q dissipative models are closer to the exact ones with increasing the series expansion order N . A similar phenomenon for the phase velocity can be found in Figures 17 through 20.

Table 1: Optimal parameters for the five-element weighting function in the frequency range $[2, 400]$ Hz, which are twice those in Table 11 of [2].

ℓ	$\tau_\sigma^{(\ell)}$ (s)	$\Delta\tau^{(\ell)} = \tau_\epsilon^{(\ell)} - \tau_\sigma^{(\ell)}$ (s)
1	9.1154190×10^{-2}	1.3759000×10^{-1}
2	1.6473674×10^{-2}	1.5164634×10^{-2}
3	4.2162695×10^{-3}	3.4910099×10^{-3}
4	1.1780240×10^{-3}	9.6118070×10^{-4}
5	2.5516913×10^{-4}	3.6195315×10^{-4}

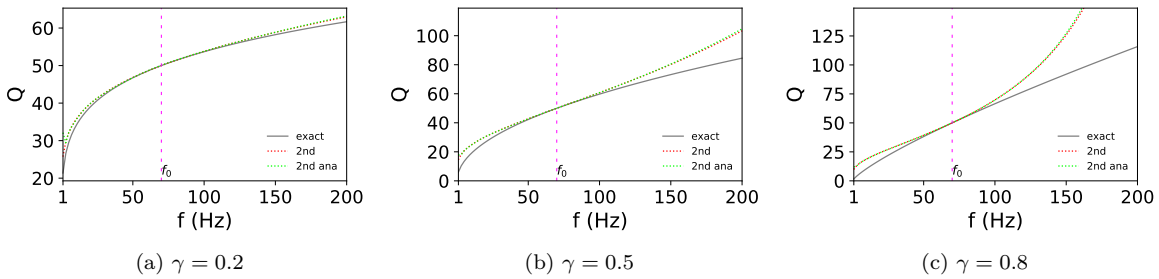


Figure 13: Variation of the quality factors with frequency. The legend label “exact” corresponds to equation 2.2 in HG2021. The legend labels “2nd” and “2nd ana” correspond to equations 2.5 and 2.14 with $N = 2$, respectively, in HG2021. The reference frequency and quality factor are $f_0 = 1$ Hz and $Q_0 = 100$, respectively.

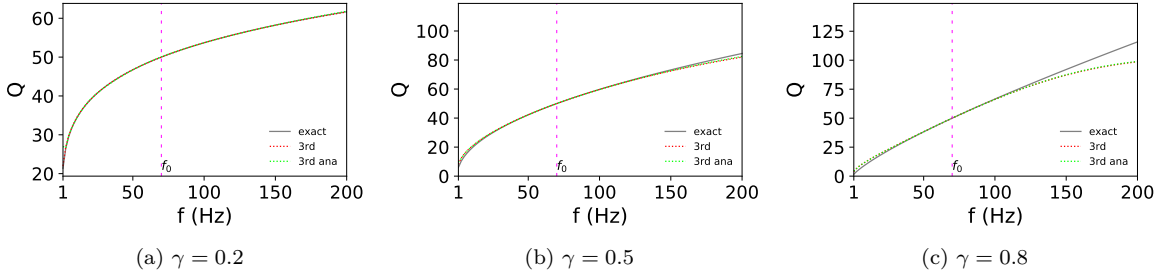


Figure 14: Similar to Figure 13 but using equations 2.5 and 2.14 with $N = 3$ in HG2021.

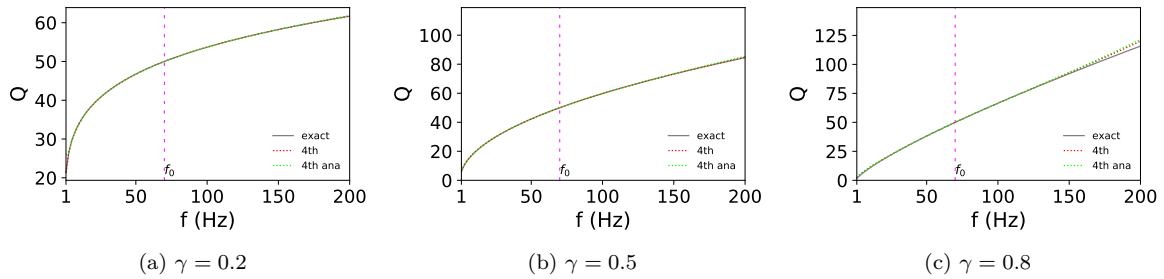


Figure 15: Similar to Figure 13 but using equations 2.5 and 2.14 with $N = 4$ in HG2021.

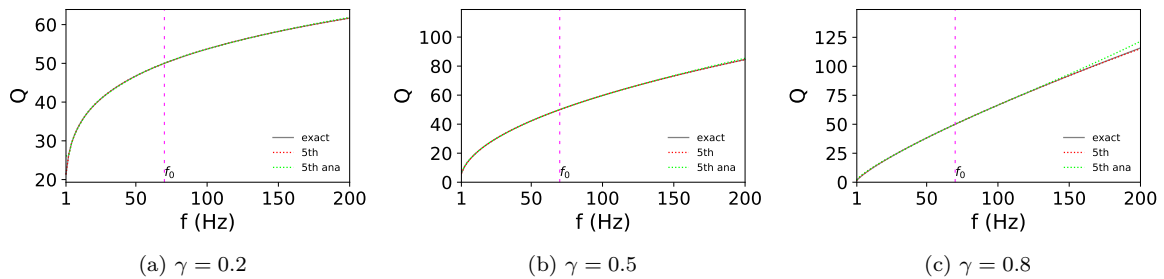


Figure 16: Similar to Figure 13 but using equations 2.5 and 2.14 with $N = 5$ in HG2021.

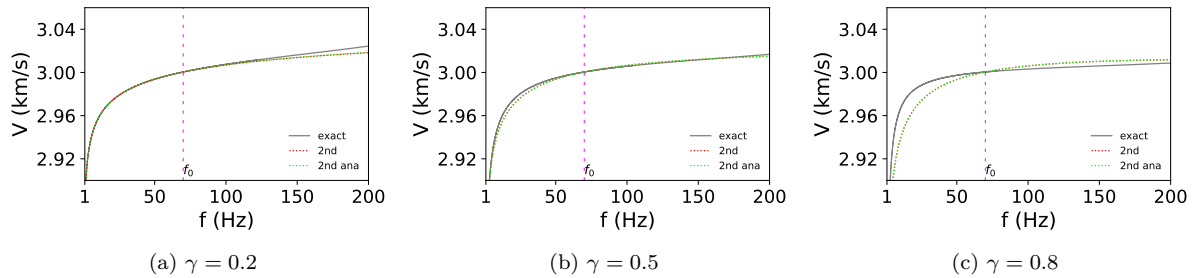


Figure 17: Variation of the phase velocity with frequency. The legend label “exact” corresponds to equation 2.2 in HG2021. The legend labels “2nd” and “2nd ana” correspond to equations 2.5 and 2.14 with $N = 2$ in HG2021, respectively.

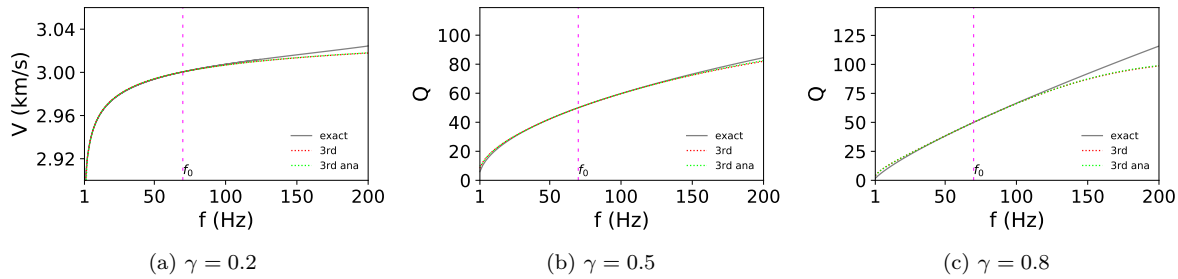


Figure 18: Similar to Figure 17 but using equations 2.5 and 2.14 with $N = 3$ in HG2021.

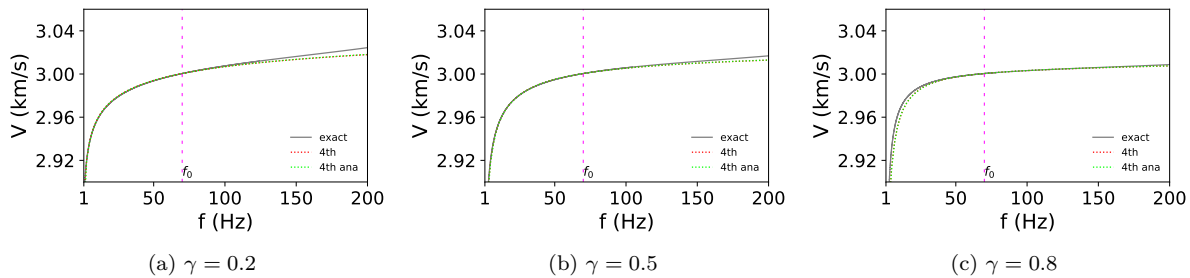


Figure 19: Similar to Figure 17 but using equations 2.5 and 2.14 with $N = 4$ in HG2021.

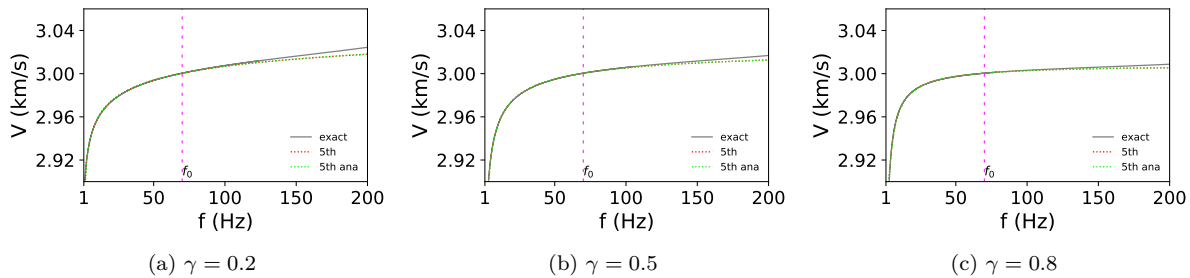


Figure 20: Similar to Figure 17 but using equations 2.5 and 2.14 with $N = 5$ in HG2021.

Numerical examples of viscoacoustic wave propagation

In the first numerical example, we investigate the viscoacoustic waveforms excited by a point source in homogeneous dissipative media. The waveforms are computed via the time-harmonic point-source viscoacoustic solution, which can be obtained from its acoustic version [3] by using the correspondence principle [4]. The reference frequency is $f_0 = 70$ Hz. The reference velocity and quality factor are $v_0 = 3$ km/s and $Q_0 = 50$. The exponent parameter γ is set as 0.2, 0.5 and 0.8 for weak, moderate and strong frequency-dependent Q , respectively. The point-source wavelet is initiated by the 70 Hz Ricker wavelet (Figure 21). The relaxation times in the weighting function are shown in Tabel 1. As illustrated in Figures 22 through 25, the waveforms for the nearly power law frequency-dependent Q dissipative models become closer to the exact ones with increasing the series expansion order N . Figures 26 through 29 show a similar phenomenon for the amplitude spectra. The nearly power law frequency-dependent Q dissipative models with $N = 5$ are accurate even for the strong frequency-dependent Q . Figures 30 and 31 show that the peak-amplitude and entire-wavelength of a viscoacoustic wave for the power law

frequency-dependent Q decrease with the exponent parameter γ . Increasing γ can delay the arrival time of the viscoacoustic wave. By comparing with the amplitude spectrum of the source wavelet (Figure 21b), Figure 30 shows that the central frequency (i.e. the frequency corresponds to the peak in an amplitude spectrum) shifts towards low frequencies and such a central frequency shift decreases with γ . However, Figure 31 shows that the effect of γ on the central frequency shift becomes negligible for $0 \leq \gamma \leq 0.4$ and a large wave-propagation distance (about 117 times the wavelength of a 70 Hz homogeneous plane wave in the same medium).

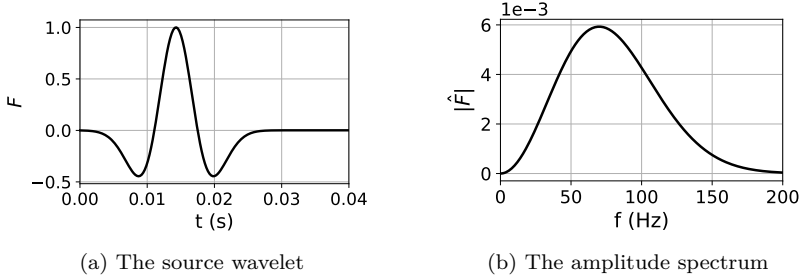


Figure 21: A 70 Hz Ricker wavelet and its amplitude spectrum.

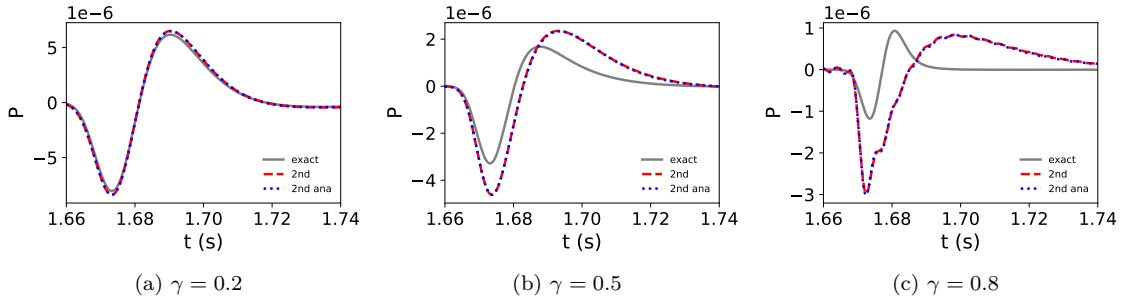


Figure 22: Viscoacoustic waveforms at a propagation distance of 5 km. The legend labels are explained in the caption of Figure 13.

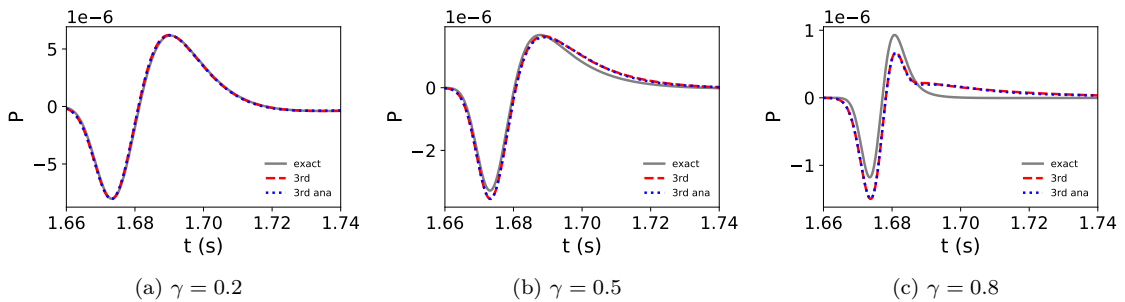


Figure 23: Similar to Figure 22 but using equations 2.5 and 2.14 with $N = 3$ in HG2021.

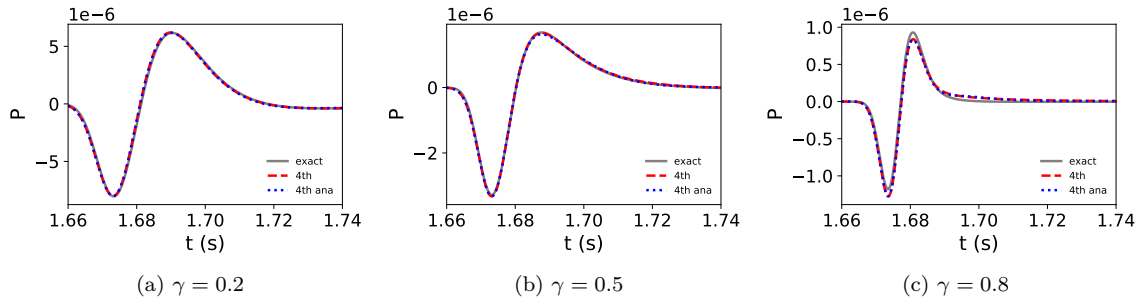


Figure 24: Similar to figure 22 but using equations 2.5 and 2.14 with $N = 4$ in HG2021.

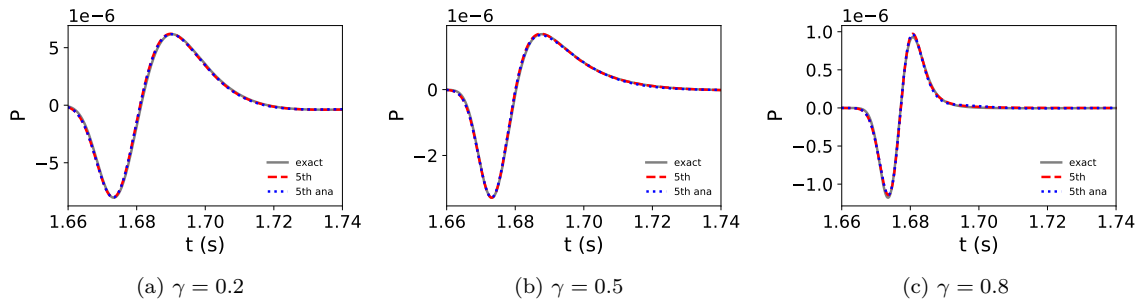


Figure 25: Similar to figure 22 but using equations 2.5 and 2.14 with $N = 5$ in HG2021.

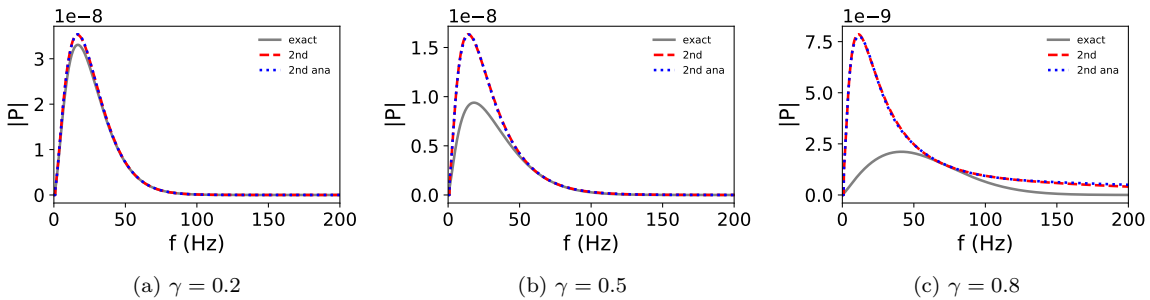


Figure 26: The amplitude spectra of the viscoacoustic waveforms in Figure 22. The legend labels are explained in the caption of Figure 13.

In the second example, we model viscoacoustic wave propagation in the Marmousi model for the power law frequency-dependent Q . The finite-difference method is implemented to numerically solve the newly proposed viscoacoustic wave equations (equations 3.2 through 3.4 of HG2021). The source term in the wave equations is initiated at the location $x = 1.645$ km and $z = 0.925$ km by a 70 Hz Ricker wavelet (Figure 21). Figure 32 shows the Marmousi model parameters defined at the reference frequency $f_0 = 70$ Hz. The reference quality factor Q_0 varies from 60 to 200, and the exponent parameter γ varies from 0.3 to 0.6. Table 1 shows the relaxation times in the weighting function. Figure 33 shows the seismograms for the acoustic ($Q_0 = \infty$), constant Q ($\gamma = 0$) and power law frequency-dependent Q versions of the Marmousi model, respectively. A comparison between these seismograms illustrates that the seismograms for the constant Q and power law frequency-dependent Q loss remarkably high-

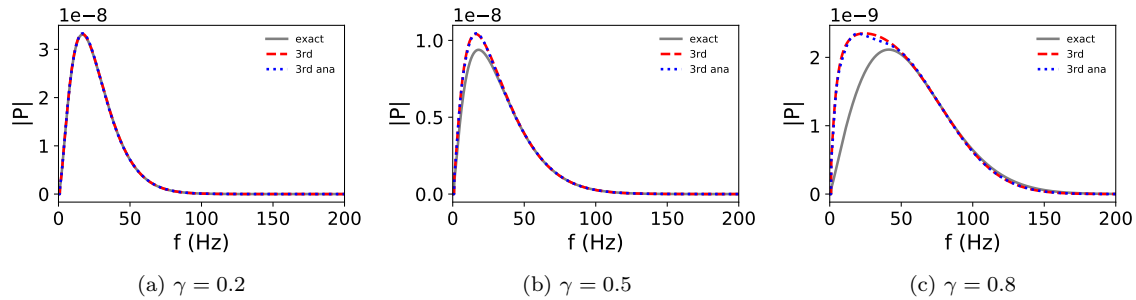


Figure 27: The amplitude spectra of the viscoacoustic waveforms shown in Figure 23. The legend labels are explained in the caption of Figure 13.

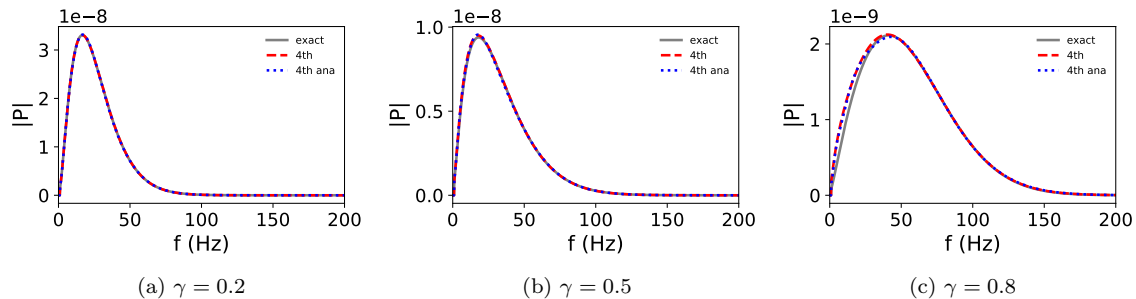


Figure 28: The amplitude spectra of the viscoacoustic waveforms in Figure 24. The legend labels are explained in the caption of Figure 13.

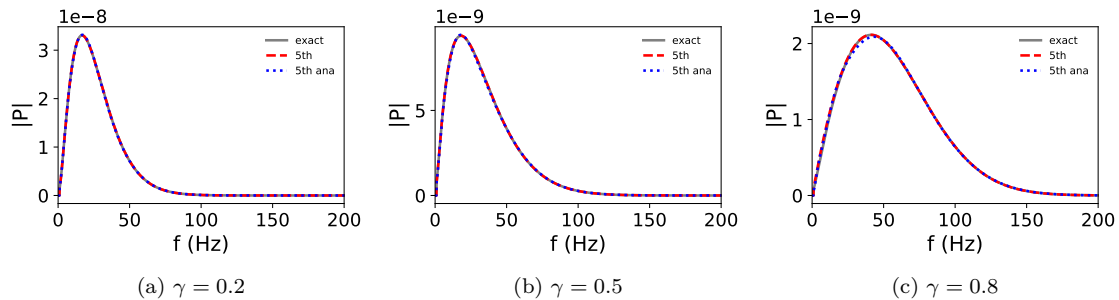


Figure 29: The amplitude spectra of the viscoacoustic waveforms in Figure 25. The legend labels are explained in the caption of Figure 13.

frequency components. Figures 34 through 42 compare single-trace seismograms extracted from Figure 33. The viscoacoustic waveforms for the constant Q and power law frequency-dependent Q are attenuated seriously due to Q . The decay of wave amplitude for the power law frequency-dependent Q is stronger than that for the constant Q , in particular for the first arrivals (e.g., Figure 34b). The wave amplitude difference between the constant Q and the frequency-dependent Q becomes apparent at receivers distant from the middle receiver ($x = 1.645$ km).

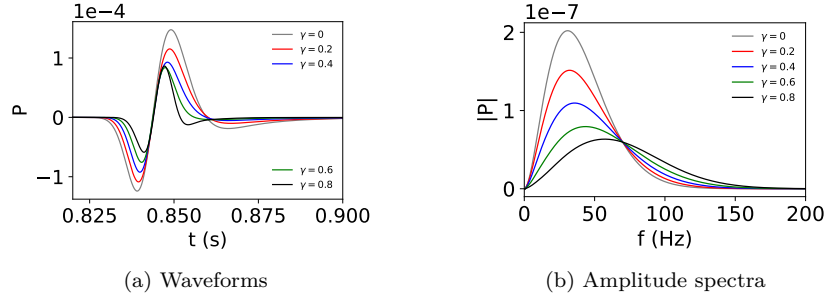


Figure 30: The effect of γ on the point-source waveforms at a wave-propagation distance of 2.5 km and their amplitude spectra. Equation 2.14 of HG2021 is used in the point-source solution to the viscoacoustic wave equation.

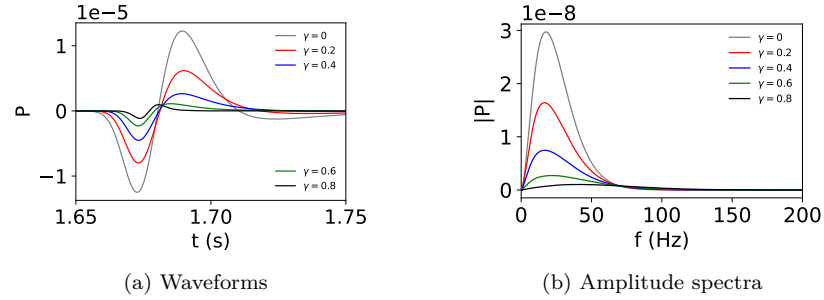


Figure 31: Similar to Figure 30 but at a wave-propagation distance of 5 km.

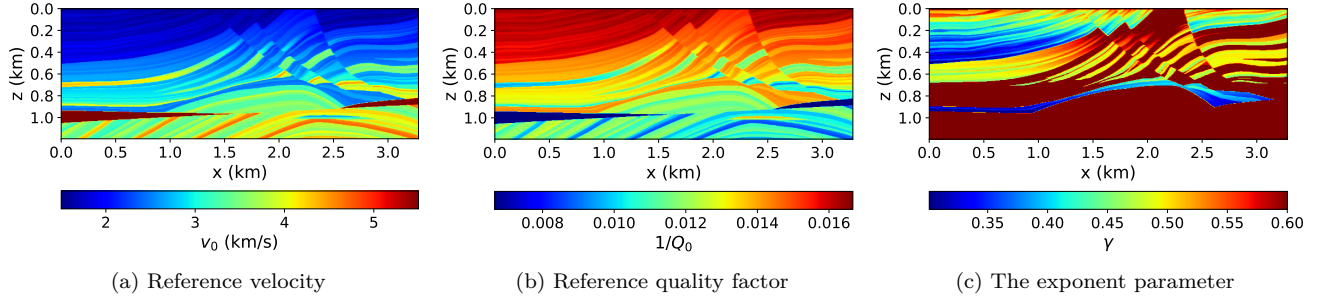


Figure 32: The Marmousi model for the power law frequency-dependent Q .

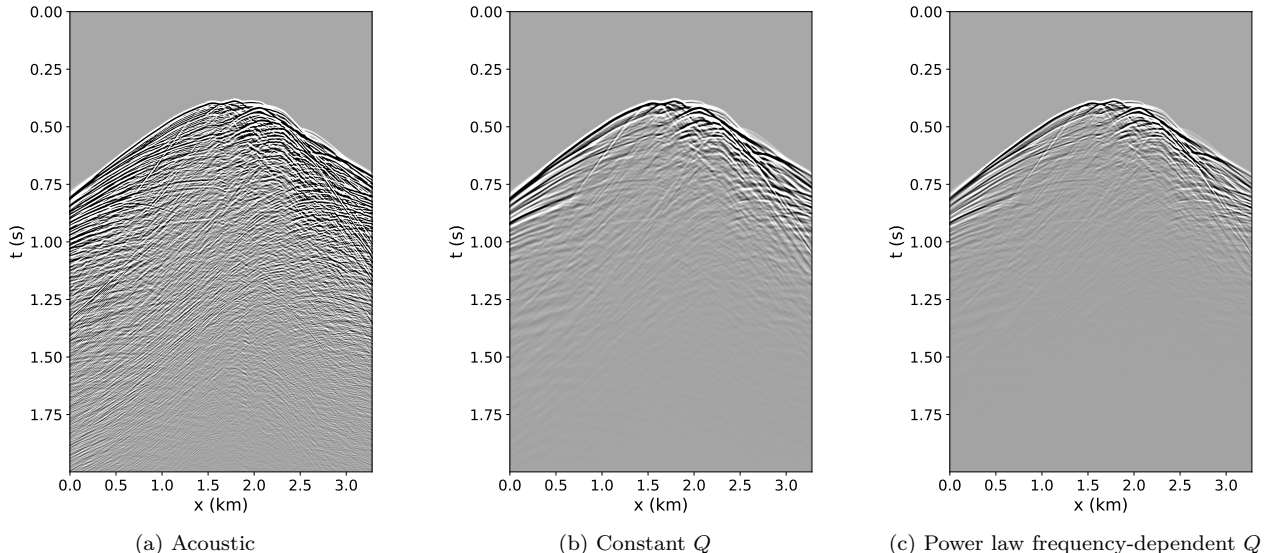


Figure 33: A comparison between the shot-gather seismograms from the acoustic, constant Q , and power law frequency-dependent Q wave equations, respectively. A gain function $t^{0.6}$ is applied to the seismograms. All the seismograms are illustrated at a same color scale.

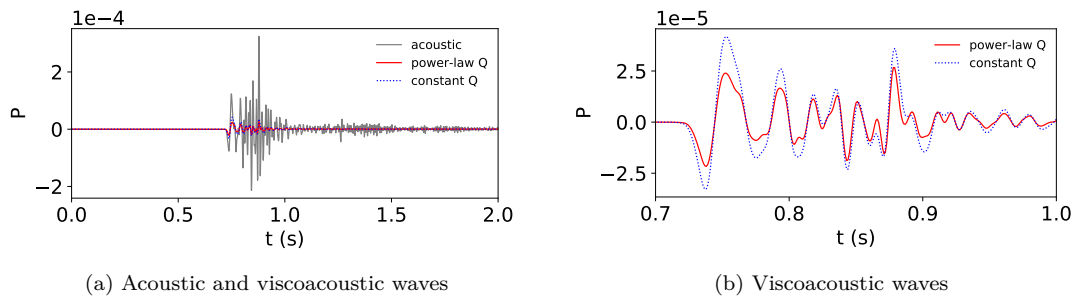


Figure 34: Single-trace seismograms for the receiver at $x = 0.2$ km. The legend labels “acoustic”, “constant Q ” and “power-law Q ” mean the acoustic ($Q_0 = \infty$), constant Q ($\gamma = 0$) and power law frequency-dependent Q cases, respectively. Plots (a) and (b) show the same viscoelastic waveforms at different illustration scales.

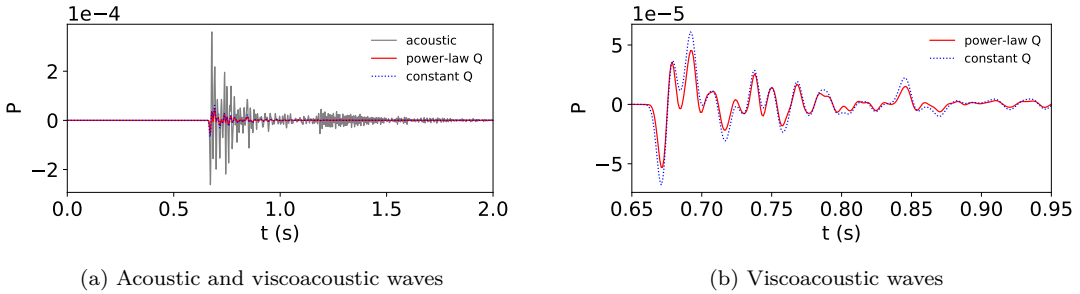


Figure 35: Similar to Figure 34 but for the receiver at $x = 0.4$ km.

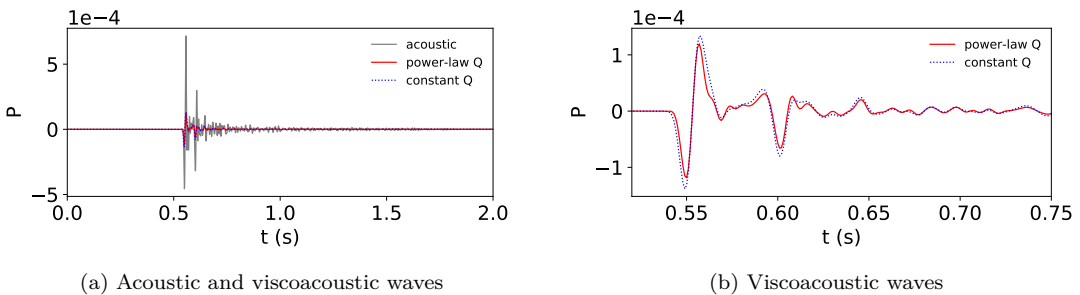


Figure 36: Similar to Figure 34 but for the receiver at $x = 0.8$ km.

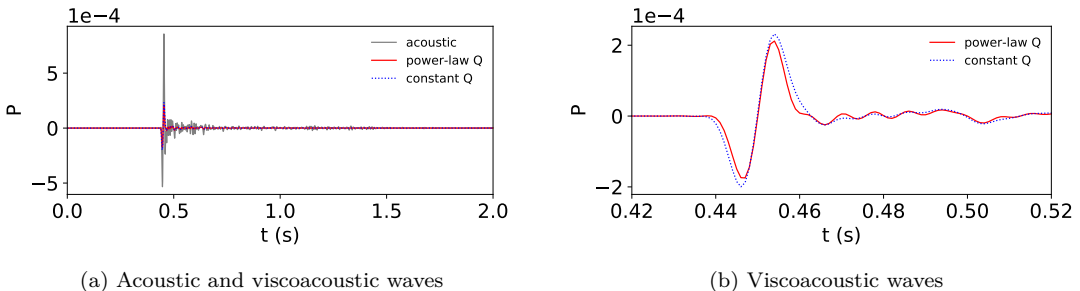


Figure 37: Similar to Figure 34 but for the receiver at $x = 1.2$ km.

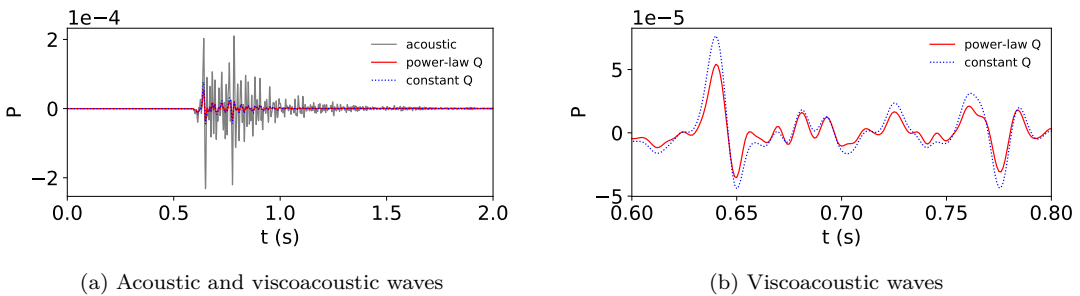


Figure 41: Similar to Figure 34 but for the receiver at $x = 2.88$ km.

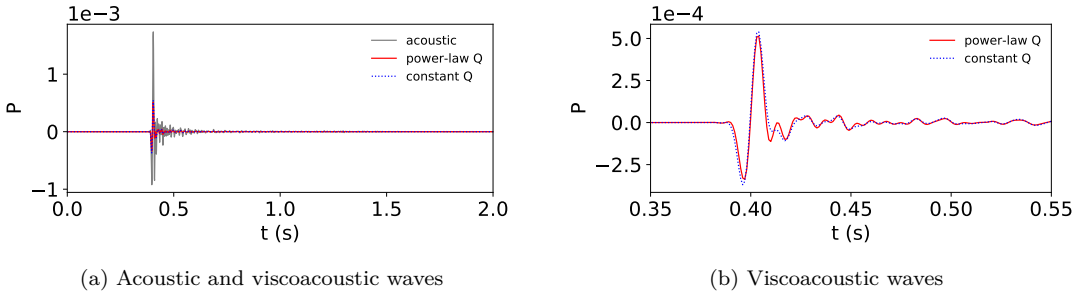


Figure 38: Similar to Figure 34 but for the receiver at $x = 1.645$ km (i.e., the middle receiver).

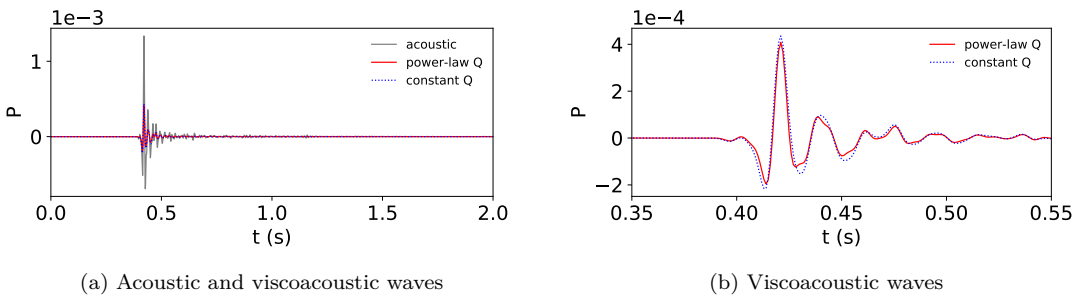


Figure 39: Similar to Figure 34 but for the receiver at $x = 2.08$ km.

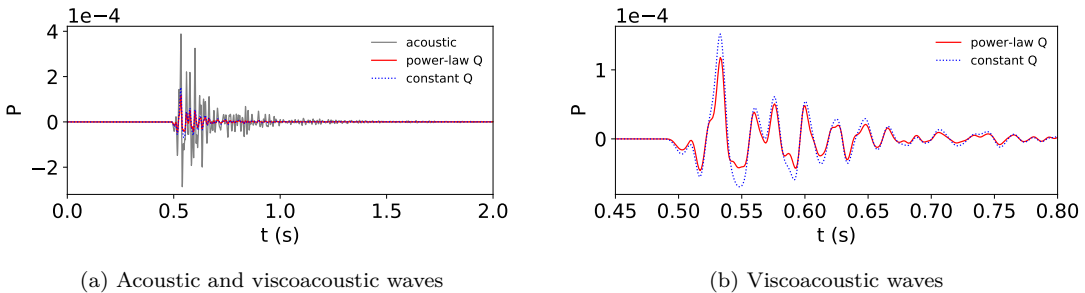


Figure 40: Similar to Figure 34 but for the receiver at $x = 2.48$ km.

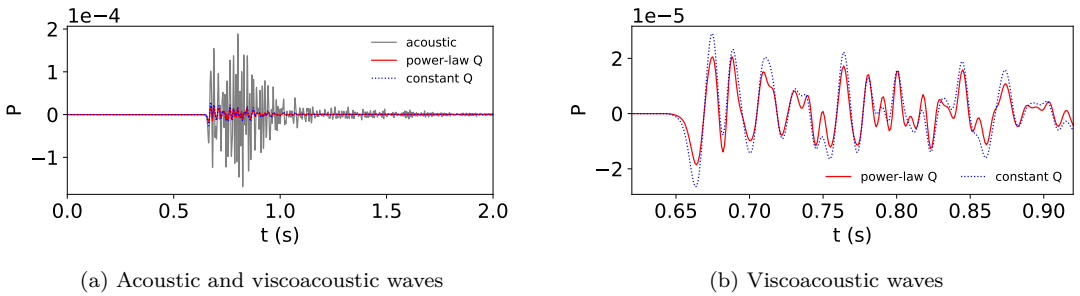


Figure 42: Similar to Figure 34 but for the receiver at $x = 2.88$ km.

Part three: explicit expressions for equations A5 through A7 of HG2021

Appendix A of HG2021 presents a method of determining the coefficients for the Maclaurin series expansion of a complex modulus from a general Q function. Equations A5 through A7 in Appendix A of HG2021 form a system of equations about the unknown coefficients a_n , $1 \leq n \leq N$. This part shows the explicit expressions for these equations with $2 \leq N \leq 5$.

For $N = 2$, equations A5 through A7 of HG2021 reduce to

$$\begin{pmatrix} f_0 & Q_0^{-1} \\ -f_1 + Q_0^{-1} & -2f_0 \end{pmatrix} \begin{pmatrix} a_1 \\ a_2 \end{pmatrix} = \begin{pmatrix} 1 \\ 0 \end{pmatrix}. \quad (1)$$

For $N = 3$, equations A5 through A7 of HG2021 reduce to

$$\begin{pmatrix} f_0 & Q_0^{-1} & -f_0 \\ -f_2 & -2f_1 + Q_0^{-1} & -3f_0 + f_2 \\ -f_1 + Q_0^{-1} & -2f_0 & f_1 - 3Q_0^{-1} \end{pmatrix} \begin{pmatrix} a_1 \\ a_2 \\ a_3 \end{pmatrix} = \begin{pmatrix} 1 \\ 0 \\ 0 \end{pmatrix}. \quad (2)$$

For $N = 4$, equations A5 through A7 of HG2021 reduce to

$$\begin{pmatrix} f_0 & Q_0^{-1} & -f_0 & -Q_0^{-1} \\ -f_2 & -2f_1 + Q_0^{-1} & -3f_0 + f_2 & 4f_1 - 6Q_0^{-1} \\ -f_1 + Q_0^{-1} & -2f_0 & f_1 - 3Q_0^{-1} & 4f_0 \\ -f_3 & -2f_2 & -3f_1 + f_3 + Q_0^{-1} & -4f_0 + 4f_2 \end{pmatrix} \begin{pmatrix} a_1 \\ a_2 \\ a_3 \\ a_4 \end{pmatrix} = \begin{pmatrix} 1 \\ 0 \\ 0 \\ 0 \end{pmatrix}. \quad (3)$$

For $N = 5$, equations A5 through A7 of HG2021 reduce to

$$\begin{pmatrix} f_0 & Q_0^{-1} & -f_0 & -Q_0^{-1} & f_0 \\ -f_2 & -2f_1 + Q_0^{-1} & -3f_0 + f_2 & 4f_1 - 6Q_0^{-1} & 10f_0 - f_2 \\ -f_4 & -2f_3 & -3f_2 + f_4 & -4f_1 + 4f_3 + Q_0^{-1} & -5f_0 + 10f_2 - f_4 \\ -f_1 + Q_0^{-1} & -2f_0 & f_1 - 3Q_0^{-1} & 4f_0 & -f_1 + 5Q_0^{-1} \\ -f_3 & -2f_2 & -3f_1 + f_3 + Q_0^{-1} & -4f_0 + 4f_2 & 10f_1 - f_3 - 10Q_0^{-1} \end{pmatrix} \begin{pmatrix} a_1 \\ a_2 \\ a_3 \\ a_4 \\ a_5 \end{pmatrix} = \begin{pmatrix} 1 \\ 0 \\ 0 \\ 0 \\ 0 \end{pmatrix}. \quad (4)$$

As elaborated in Appendix A of HG2021, f_n for $n > 1$ can be determined for a specified Q function except that f_0 is set as $f_0 = 1$. This is also true for the power law frequency-dependent Q function. Substituting the expressions for f_n into the above equations about a_n for a specified N and solving the resulting equations gives rise to the coefficients for the Maclaurin series expansion of the complex modulus for the power law frequency-dependent Q . In this case, explicit expressions for a_n are given in HG2021 by equations 2.6 and 2.7 for $N = 2$, equations 2.8 through 2.10 for $N = 3$, equation B2 together with equations B3 through B7 for $N = 4$, and equation B2 together with equations B8 through B13 for $N = 5$.

References

- [1] G. Muller, Rheological properties and velocity dispersion of a medium with power-law dependence of Q on frequency, *Journal of Geophysics* 54 (1) (1983) 20–29.
- [2] Q. Hao, S. Greenhalgh, Nearly constant Q models of the generalized standard linear solid type and the corresponding wave equations, *Geophysics* 86 (4) (2021) T239–T260.

- [3] J. Pujol, Elastic wave propagation and generation in seismology, Cambridge University Press, 2003.
- [4] J. M. Carcione, Wave fields in real media: Theory and numerical simulation of wave propagation in anisotropic, anelastic, porous and electromagnetic media: Handbook of Geophysical exploration (3rd ed.), Elsevier, 2014.